The role of activity, scan duration and patient's weight in the optimization of 18FDG imaging protocols on a TOF-PET/CT scanner

Roberta Matheoud (roberta.matheoud@maggioreosp.novara.it)
Azienda Ospedaliero-Universitaria Maggiore della Carita https://orcid.org/0000-0002-4783-0744
Naema Al-Maymani
Abdus Salam International Centre for Theoretical Physics
Alessia Oldani
Universita del Piemonte Orientale Amedeo Avogadro Biblioteca Norberto Bobbio
Gian Mauro Sacchetti
Azienda Ospedaliero-Universitaria Maggiore della Carita
Marco Brambilla
Azienda Ospedaliero-Universitaria Maggiore della Carita
Alessandro Carriero
Azienda Ospedaliero-Universitaria Maggiore della Carita

Original research

Keywords: Positron emission tomography, time-of flight, 18FDG, Contrast-to-noise ratio, optimization, image quality

Posted Date: March 23rd, 2020

DOI: https://doi.org/10.21203/rs.3.rs-17743/v1

Abstract

Background : Time-of-flight (TOF) PET technology determines a reduction in the noise and improves the reconstructed image quality , in low counts acquisitions, such as in overweight patients, allowing a reduction of administered activity and/or imaging time. However, international guidelines and recommendations on 18 F-fluoro-2-deoxyglucose (FDG) activity administration scheme are old or only partially account for TOF technology and advanced reconstruction modalities.

The aim of this study was to optimize FDG whole-body studies on a TOF PET/CT scanner by using a multivariate approach to quantify how physical figures of merit related to image quality change with acquisition/reconstruction/patient-dependent parameters in a phantom experiment.

Methods : The NEMA-IEC body phantom was used to evaluate contrast recovery coefficient (CRC), background variability (BV) and contrast-to-noise ratio (CNR) as a function of changing emission scan duration (ESD), activity concentration (AC), target internal diameter (ID), target-background activity ratio (TBR), and weight. The phantom was filled with 5.3 kBq/mL of FDG solution and the spheres with TBR of 21, 9, and 5 in 3 different sessions. Images were acquired at varying activity concentration from 5.1 to 1.3 kBq/mL and images were reconstructed for ESD of 30-151 seconds per bed position with and without Point Spread Function (PSF) correction. The parameters were all considered in simultaneous experiments and in a single analysis using multiple linear regression methods.

Results : As expected, CRC depended only on sphere ID and on PSF application, while BV depended on sphere ID, ESD, AC and weight of the patient, in order of decreasing relevance. Noteworthy, ESD and AC resulted as the most significant predictors of CNR variability with a similar relevance, followed by the weight of the patient and TBR of the lesion.

Conclusions : Due to the interchangeable role of AC and ESD in modulating CRC, ESD could be increased rather than AC to improve image quality in overweight/obese patients to fulfil ALARA principles.

Background

Thanks to the improvements in hardware components and in imaging reconstruction techniques, significant advances have been made in recent years in positron emission tomography / computed tomography (PET/CT) systems [,]. They are mainly related to the use of fast detectors, Lutetium Oxyorthosilicate (LSO) and/or Lutetium Yttrium Oxyorthosilicate (LYSO) coupled to both Time-of-Flight (TOF) technology and advanced reconstruction modalities such as the modelling of the system Point-Spread-Function (PSF) [,,] and/or noise [] which improve the accuracy of quantitative information and enhance the detectability of small lesions [,].

The main motivation for TOF-PET has always been the potential image quality improvement or reduction in image acquisition time [1,2]. The effective sensitivity gain was already described nearly 40 years ago [8,] as depending on the ratio between the object size D and the spatial FWHM of the TOF kernel Δx.

In oncology practice, typically a longer acquisition time is needed for a larger patient characterized by higher attenuation. Often the longer acquisition time does not compensate for the poor quality of the data. Because of the higher attenuation, larger patients are affected by more noise. TOF acts as an equalizer, bringing the image quality in larger patients closer to that in patients of average size [,]. Thus, the first consequence of TOF technology is that SNR gain is increased, and this is especially more evident for larger patients [2,].

This improvement has been used in the clinical setting predominantly to reduce the imaging time [1,2].

However, international guidelines and recommendations on FDG activity administration scheme are rather old [] or only partially account for time-of-flight technology [] and advanced reconstruction modalities. Therefore, precise information on how to tune administered FDG activity and emission scan duration in whole-body oncological studies on TOF-PET/CT scanners, is still a demanding need for the nuclear medicine physicians.

Few papers in the literature studied the optimization of ^{18}FDG activity administration [,] or emission scan duration [] on TOF-PET/CT scanners, but they examined the two factors independently.

The aim of this work was to describe how the physical figures of merit related to PET image quality change with different acquisition, reconstruction and object dependent parameters on a TOF-PET/CT scanner. The study was designed to simultaneously analyse the impact of the different factors with a multivariable approach, using phantoms with a variable weight, which hosted several well-defined target sizes with a known target-to -background ratio, as done in previous study []. We selected the emission scan duration (ESD), the FDG activity concentration (AC), the target-to-background activity concentration ratio (TBR), the target size (ID), the weight (W) of scanned object and the application of PSF correction (PSF) as the factors that could affect the Contrast Recovery Coefficient (CRC), the Background Variability (BV) and the Contrast-to-Noise Ratio (CNR), identified as PET image quality descriptors.

Methods

PET/CT scanner

The Ingenuity TF 64 PET/CT scanner (Philips Healthcare, Cleveland, OH, USA) is equipped with 28336 Lutetium-Yttrium Oxyorthosilicate (LYSO) detectors and TOF technology. The PET ring diameter is 90 cm with an axial Field of View (FOV) of 18 cm. The 28 modules are organized in 23 by 44 matrices of 4 × 4 × 22 mm3 LYSO crystal coupled to 420 hexagonal photomultiplier tubes with the PIXELAR detector design and a continuous light guide. Data are exclusively acquired in a three-dimensional (3D) list-mode format. The energy window is set between 440 and 665 keV. The standard reconstruction transverse FOV is 576 mm for standard whole-body patient acquisitions. The coincidence window is 3.8 ns. The CT component is a 64-slice scanner with a 4 cm axial coverage. The performance characteristics of this TOF-PET/CT scanner according to NEMA NU 2012 standard have already been described in detail [].

Phantom setup

The NEMA International Electrotechnical Commission (IEC) Body Phantom with ^{18}F solution was used. The IEC phantom has an interior cavity volume of 9947 mL and contains 6 fillable spheres with 10, 13, 17, 22, 28, and 37 mm inner diameters (ID). A cylindrical insert filled with low density foam (density of 0.30 g/cm^3) was fixed along the centre of the phantom. Four micro-hollow spheres with ID of 4.1, 4.7, 6.5, and 8.1 mm were fixed to a foam support attached to the lung insert at the bottom of the phantom. The IEC phantom was centred in the transverse FOV of the scanner with the equatorial plane of the standard spheres coplanar to the centre of the axial FOV.

To simulate the activity outside the scanner FOV, the scatter phantom (Data Spectrum Corporation) was placed close at the end of the IEC phantom. It is a solid circular cylinder composed of polyethylene with outside diameter of 203 mm and a length of 700 mm. A 6.4 mm hole is drilled along central axis of the cylinder. A 700 mm polyethylene tube with an inside diameter of 3.2 mm and an outside diameter of 4.8 mm is placed in the hole.

Finally, to simulate a different patient habitus (W), a belt of 11 water bags of 500 mL and 3 cm thick was fit over the IEC phantom, resulting in an additional weight of 5.5 kg. Thus, while the IEC phantom simulates the standard 70 kg weight man, the IEC fitted with the additional belt represents a 108.5 kg weight man.

Phantoms preparation and acquisition

The spheres of the IEC phantom were filled with ^{18}F activity concentrations of 25.6, 46.6 and 117.3 kBq/ml and the IEC cavity with ^{18}F activity concentration of 5.1, 5.3 and 5.5 kBq/ml, in three different experimental sessions, respectively, thus providing 21, 9 and 5 target-to-background ratios (TBR). The reference time for all the activity concentrations is the time of the first acquisition, as described in the paragraph below.

A more clinical parameter used to evaluate the uptake in a lesion is the Standardize Uptake Value (SUV) which describes the activity concentration in the lesion with respect to the total activity concentration in the phantom (this last being normally higher than the background concentration). The correspondent SUV values realized in the three experimental sessions were 19, 8 and 5, respectively.

The capillary present in the scatter phantom was filled with ^{18}F activity concentrations of 5.3, 5.1, 5.3 kBq/ml in the three experimental sessions, respectively.

PET/CT images of both IEC and IEC wrapped with the belt (b-IEC) were acquired in list mode with the NEMA NU-2 2012 protocol with one bed of 151 sec to simulate a total body scan of 100 cm axial imaging distance in 30 minutes of emission imaging and in accordance to the manufacturer's protocol []. IEC and b-IEC phantoms were acquired sequentially, at different activity concentrations of about 5.1, 3.1, 2.2, 1.5

and 1.3 kBq/ml. Overall 30 (5 activity concentrations x two phantoms x 3 replicates) acquisitions were performed. A CT scan was used for attenuation correction.

Image reconstruction

After correction for attenuation, scatter, random, detector normalization, isotope decay, system dead time and crystal timing, images were reconstructed using a TOF, list-mode, blob-based, ordered subsets maximum likelihood expectation maximization algorithm (TOF-OSEM) [].

The standard protocol provided by the manufacturer for clinical whole body examinations was used to reconstruct all the images acquired, by setting the Speed to Normal (99 equivalent iterations and a TOF kernel width of 14.1 cm), the Smooth to Normal (amplitude of the Gaussian filter equal to 4 mm and the relaxation parameter equal to 1.0) on a 144 × 144 frame (4 mm isotropic voxel). The reconstructions were performed for different emission scan durations (ESD) with and without the application of the resolution recovery algorithm or PSF correction (PSF) as shown in Table 1. The PSF, speed and smoothing filter parameters were kept fixed for each reconstruction, as we demonstrated previously that no significant difference in contrast recovery coefficient and background variability exists by changing speed, smooth and PSF values [19].

Table 1
Reconstruction parameters values used in phantom image reconstruction

Reconstruction parameter	Values
ESD (sec)	30, 45, 60, 75, 90, 120 and 151
PSF correction (on/off)	1 iteration, 6 mm regularization
Speed Normal	3 iterations, 33 subsets
Smooth Normal	4 mm Gaussian filter amplitude

Image analysis

The percentage Contrast Recovery Coefficient (CRC) and the Background Variability (BV) were evaluated by a routine provided by the manufacturer, according to NEMA NU-2 2012 standards.

Moreover, the contrast-to-noise ratio (CNR), which is the physical figure of merit more closely related to lesion detectability, was evaluated for all the spheres that were detected on the reconstructed images, by using the following formula [18]:

$$\mathrm{CNR} = \frac{(C_S - C_B)/C_S}{SD_B/C_B}$$

where C_S is the average counts in the ROI for sphere S, C_B and SD_B the mean and standard deviation of the mean of all background ROIs drawn for the BV evaluation, namely 600 background ROIs (10 spheres x 12 positions x 5 slices). Overall, 4200 data were analysed.

Statistical Analysis

Correlation matrices were used to identify potential univariate correlations between image quality figures of merit (CRC, BV and CNR) and acquisition (ESD, AC), reconstruction (PSF application) and object dependent parameters (ID, TBR and W). Only significant predictors at univariate analysis were considered and inserted into multiple linear regression methods to derive analytical formulas of the model.

The weight of different dependent variables in explaining the independent variables were quantified by means of standardized regression coefficients. The standardized regression coefficients can be used as a measure of relative importance, with the independent variables ranked in order of the sizes of these coefficients (ignoring sign) [].

Box and whiskers plots were used to provide a univariate graphical representation CRC and BV with respect to significant predictors, identified by the regression models. Outliers and extremes are points higher than the value of the 75th percentile plus 1.5 or 3 times the interquartile distance, or lower than the value of the 25th percentile minus 1.5 or 3 times the interquartile distance, respectively.

The impact of the different acquisition and object dependent parameters on CNR, was further investigated by a multiple way principal effects ANOVA: acquisition and object dependent parameters were considered as independent variables (factors) and CNR as the dependent variables A post-hoc test (Scheffe´ F test) was performed to identify the main sources of variability. If a significant F value was found for one independent variable, then this was referred as a main effect. When a main effect was found, then the Scheffe´ test was performed to compare the dependent variable upon the levels of the factor 2 × 2, thus identifying the main sources of variability. These comparisons were represented by drawing the least squares means, which are the best linear estimates for the marginal means in the ANOVA design, together with the standard errors of the means (and thus the 95% confidence intervals). The statistical analysis was performed with the software STATISTICA 6.0 (Statsoft Inc, USA).

Results

Contrast recovery coefficient

The recovery of ^{18}F activity in the spheres of IEC phantom depends on sphere ID ($\beta_{ID} = 0.68$) and on the application of PSF correction ($\beta_{PSF} = 0.23$), in order of decreasing relevance of the weight of the variable in the model (β). The adjusted R^2 of model fitting was 0.51.

The multiple linear regression equation that summarizes the model with CRC as predicted variable and sphere ID and PSF-IT as predictors can be written as:

$$CRC = 20.8 + 1.8 * sphereID + 11.8 \text{ x } PSF \quad (1)$$

Background variability

The multiple linear regression analysis showed that BV depends on sphereID (β_{ID}=-0.62), ESD (β_{ESD}=-0.39), AC (β_{AC}=-0.31) and W (β_W = 0.24), in order of decreasing relevance. The adjusted R^2 of model fitting equals to 0.77. The multiple linear regression equation that summarizes the model with BV as predicted variable and sphere ID, ESD, AC and W as predictors can be written as:

$$BV = 26.1 - 0.5 * sphereID + 0.1 * ESD - 1.9 * AC + 0.7xW \quad (2)$$

Contrast to noise ratio

The CNR of the spheres detected on the images depends on ESD (β_{ESD} = 0.53), AC (β_{AC} = 0.51), W (β_W=-0.38) and TBR (β_{ESD} = 0.26), in order of decreasing relevance. The adjusted R^2 of model fitting equals to 0.76. The regression equation that best summarizes the results obtained in a multiple regression model for CNR is:

$$CNR = 3.96 + (0.03 \text{ x } ESD) + (0.74 \text{ x } AC) - (0.28 \text{ x } W) + (0.08 \text{ x } TBR) \quad (3)$$

ESD and AC impact with a similar weight on CNR, As expected, W impacts with a negative regression coefficient on CNR, i.e. as the weight increases the CNR decreases. Only last came TBR, with a slight impact on CNR about one half the one of ESD and AC. Post-hoc Scheffè test showed a statistically significant increase in CNR for every contrast between adjacent levels of AC in the range explored ($p < 0.001$) (Fig. 3a). When considering 2.2 kBq/mL, which represents the activity concentration 60 minutes post injection of 3 MBq/kg of 18F-FDG, the CNR mean value increases of about 19% when moving to an activity concentration of 3.1 kBq/mL (which correspond to an injection scheme of 4.5 kBq/ml).

A similar behaviour was observed for all the ESD, W and TBR contrast tested. Post-hoc Scheffè test showed a statistically significant increase in CNR for every contrast between adjacent levels of ESD (Fig. 3b), weight (Fig. 3c) and TBR (Fig. 3d) in the range explored ($p < 0.001$).

Discussion

Precise information on how to tune acquisition and reconstruction parameters as well as FDG activity to administer to patients in whole-body oncological studies on TOF-PET/CT scanners is required to balance the improvement in the image quality with the opportunity of reducing the radiation dose burden in particular to patients frequently exposed to several radiological examination during their follow up, as part of the optimization process required by the Euratom Directive 2016-59 [23].

The image quality and lesion detectability in ^{18}F-FDG PET imaging are limited by the low signal-to-noise ratio and by the relatively low spatial resolution, which results in a partial-volume effect affecting lesion visualization and quantitation [2].

This work was aimed to characterize the quality of PET images for a TOF-PET/CT scanner in a wide range of acquisition, reconstruction and object dependent parameters in settings like those encountered in clinical practice, by means of a phantom study. CRC, BV and CNR, which is closely related to lesion detectability, were the figures of merit used to describe PET image quality. Our study used a multivariate approach to quantify how these figures of merit change as a function of ESD and AC for different target size, TBR, weight and under the effect of the point spread function modelling correction.

The main result of this study is that the CNR of FDG lesions depends on ESD and AC in a similar way (β = 0.53 and β = 0.51). This result is rather new: a previous study performed on a non-TOF PET scanner [18] concluded that the main predictor of CNR was ESD (β = 0.60) and only with a half of the explanatory power (β = 0.27) came AC.

Moreover, our results show also a significant increase in CNR for each increasing step in AC or ESD in the range explored, i.e. from 1.3 to 5.0 kBq/ml and from 30 to 151 sec. The visual inspection of phantom images confirmed that the image quality, in terms of the noise level and contrast, can be improved by increasing the AC (Fig. 4a) or ESD (Fig. 4b). This finding agrees with the clinical results reported in the recent paper of Prieto [16]. The author observed a statistically significant difference in both the image noise and the overall image quality indexes of PET images obtained after 18FDG activity administration of 5.2 and 3.7 MBq/kg on the Siemens mCT TOF-PET/CT scanner.

The third predictor of CNR was the weight of the phantom (β=-0.38), indicating that on average the CNR decreased by 28% with increasing the weight of the scanned object by a factor of 1.55. It is known that the TOF technology allowing the reduction of the uncertainty on the annihilation event acts as a noise equalizer and brings an overall gain in signal-to noise ratio, being this effect more evident for larger object [1, 10]. However, our result is quite new, at least to our knowledge, and shows that notwithstanding the TOF technology, there is still a dependence of CNR on the weight of the imaged object. This means that there is an additional way to improve the lesion detectability for larger patients, depending on their weight. This result suggests the definition of specific acquisition protocols for oncological whole-body studies tailored on patient's habitus, rather than using a fixed ESD of 60 seconds per bed position, as suggested by the manufacturer.

The last predictor of CNR was the TBR of the lesion (β = 0.26). This dependence may be explained by the partial volume effect, which reduces the apparent activity concentration in the lesion in the reconstructed image preventing the recovering of the true amount of activity for structures less than twice the reconstructed image resolution. The major gain in CNR was observed for low TBR (or low SUV) values, as when moving from TBR 5 to 9 the CNR increases of about 19%, while when moving from TBR 9 to 21 the

CNR increase is only of about 9% (Fig. 3d). However, this is an intrinsic characteristic of the lesion itself and cannot be managed in the optimization process.

The fitted multiple regression model of CNR based on these premises, accounts for more than two thirds of CNR variance (adjusted $R^2 = 0.76$).

From these findings, one can derive that it is possible to opportunely tune ESD and AC on patient's weight in order to keep constant the CNR, or the detectability level, on the PET images of this scanner.

As a typical example, let us consider the following situation: a lesion with a TBR of 9 (SUV = 8.8) in a standard 70 kg body weight patient injected with 3 MBq/kg of ^{18}F-FDG imaged for 60 sec, 60 minutes post injection. According to Eq. (3), we should expect a CNR of 5.2. To obtain a similar value in CNR for the same lesion uptake in an obese 108 kg body weight patient injected with 3 MBq/kg of 18F-FDG, the patient should be scanned for 120 s. In an analogous way, one could double the activity administration scheme (i.e. 6 MBq/kg) to obtain the same CNR. However, from a radiation protection point of view, it would be more advisable to increase the ESD than the AC for an improvement in lesion detectability.

Another result of this study is the dependence of CRC on sphere ID ($\beta = 0.68$) and PSF application ($\beta = 0.23$). This result confirms the dependence of CRC already reported by Zorz et al. [19], even with a slightly different analytical expression with respect to (2). This may be explained by observing that in [19] only four spheres (ID = 10,13,17 and 22 mm) were included in NEMA-IEC phantom analysis and CRC fitting was almost perfectly linear (R_{adj}^2=0.93). In our study, on the contrary, CRC dependence on ID was analysed in a wider sphere dimension range, where CRC values assume a sigmoidal trend with respect to ID (Fig. 1a), explaining also the relatively low R_{adj}^2 of 0.51.

The third parameter related to image quality we investigated, the BV resulted to be dependent on the ROI dimension for which is defined (β=-0.62), emission scan duration (β=-0.39), activity concentration (β=-0.31) and weight ($\beta = 0.24$), in order of decreasing relevance, this model explaining 77% of variance in BV (R_{adj}^2 of 0.77). The strong dependence of BV on sphere ID is not new and was also found by Zorz [19] and Brambilla [18], with similar weights. Even if BV cannot be considered a descriptor of noise, it is interesting to note the equivalent dependence of BV on ESD (β = -0.39) and AC (β = -0.31), in analogy with the finding that CNR depends on both these parameters with similar weights, reported above. The impact of the weight of the phantom on BV, actually reinforces the same finding on CNR.

A limitation of this study must be acknowledged: the results on CRC, BV and CNR found in the present study strictly apply to this PET/CT scanner and to FDG oncological examinations: extrapolation of these results to different TOF-PET/CT scanners and to different radionuclides should be tested in advance before application.

Abbreviations

TOF

Time-of-flight
FDG
^{18}F-fluoro-2-deoxyglucose
PET
Positron Emission Tomography
CT
Computed Tomography
CRC
Contrast Recovery Coefficient
BV
Background Variability
CNR
Contrast to Noise Ratio
ESD
Emission Scan Duration
AC
Activity Concentration
ALARA
As Low As Reasonably Achievable
ID
Internal Diameter
TBR
Target-Background activity Ratio
W
Weight
LSO
Lutetium Oxyorthosilicate
LYSO
Lutetium Yttrium Oxyorthosilicate
PSF
Point Spread Function
FWHM
Full Width at Half Maximum
NEMA
National Electrical Manufacturer Association
IEC
International Electrotechnical Commission
b-IEC
IEC phantom wrapped with belt
OSEM

Ordered Subset Expectation Maximization

Declarations

Ethics approval and consent to participate
Not applicable

Consent for publication
Not applicable

Availability of data and material
The datasets used and analyzed during the current study are available from the corresponding author on reasonable request.

Competing interests
The authors declare that they have no competing interests.
Funding
Not applicable

Authors' contributions
RM, MB and AC contributed to the design of the study. RM, NAM and AO performed the data acquisition with the support from GMS. NAM and AO reconstructed and analysed the images. RM drafted this paper, which was revised by MB and GMS. All authors approved the final manuscript.

Acknowledgements
Not applicable

References

1. Vandenberghe S, Mikhaylova E, D'Hoe E, Mollet P, Karp JS Recent developments in time-of-flight PET. EJNMMI Phys. 2016 Dec;3(1):3. doi: 10.1186/s40658-016-0138-3
2. Van der Vos CS, Koopman D, Rijnsdorp S et al. Quantification, improvement, and harmonization of small lesion detection with state-of-the-art PET. Eur J Med Mol Imaging 2017; 44(Suppl 1): S4-S16.
3. Lecomte R, Schmitt D, Lamoureux G. Geometry study of a high resolution PET detection system using small detectors. IEEE Trans Nucl Sci 1984;31:556-61
4. Alessio AM, Kinahan PE, Lewellen TK. Modeling and incorporation of system response functions in 3-D whole body PET. IEEE Trans Med Imaging 2006;25: 828-37.
5. Panin VY, Kehren F, Michel C, Casey M. Fully 3-D PET reconstruction with system matrix derived from point source measurements. IEEE Trans Med Imaging 2006;25:907-21.
6. Teoh EJ, McGowan DR, Macpherson RE, Bradley KM, Gleeson FV. Phantom and clinical evaluation of the Bayesian penalized likelihood reconstruction algorithm Q.Clear on an LYSO PET/CT system. J

Nucl Med 2015;56(9):1447–52. doi:10.2967/jnumed.115.159301

7. Rahmim A, Tang J. Noise propagation in resolution modeled PET imaging and its impact on detectability. Phys Med Biol 2013;58:6945-68.
8. Knäusl B, Rausch IF, Bergmann H, Dudczak R, Hirtl A, Georg D. Influence of PET reconstruction parameters on the TrueX algorithm. A combined phantom and patient study. Nuklearmedizin 2013;52: 28-35.
9. Budinger TF Time-of-flight positron emission tomography: status relative to conventional PET. J Nucl Med. 1983;24:73-8
10. Conti M Focus on time-of-flight PET: the benefits of improved time resolution, Eur J Nucl Med Mol Imaging (2011) 38:1147–1157. DOI 10.1007/s00259-010-1711-y
11. Karp JS, Surti S, Daube-Witherspoon ME, Muehllehner G. Benefit of Time-of-Flight in PET: experimental and clinical results. J Nucl Med 2008;49:462-470
12. Lois C, Jakoby BW, Long MJ et al. An assessment of the impact of incorporating Time-of-Flight information into clinical PET/CT imaging. J Nucl Med 2010;51:237-245.
13. Delbeke D, Coleman RE, Guiberteau MJ, Brown ML, Royal HD, Siegel BA, et al. Procedure guideline for tumor imaging with 18F-FDG PET/CT 1.0. J Nucl Med 2006;47:885–95.
14. Boellaard R, Delgado-Bolton R, Oyen WJG, Giammarile F, Tatsch K, Eschner W, et al. FDG PET/CT: EANM procedure guidelines for tumour imaging: version 2.0. Eur J Nucl Med Mol Imaging 2015;42:328–54.
15. Schaefferkoetter J, Nai YH, Reilhac A et al. Low dose positron emission tomography emulation from decimated high statistics: A clinical validation study. Med. Phys. 2019;46:2638-2645.https://doi.org/10.1002/mp.13517
16. Prieto E, Garcia-Velloso MJ, Rodriguez-Fraile M, et al. Significant dose reduction is feasible in FDG PET/CT protocols without compromising diagnostic quality. Phys Med. 2018 Feb;46:134-139. doi: 10.1016/j.ejmp.2018.01.021.
17. Murray I, Time-of-flight PET/CT using low-activity protocols: potential implications for cancer therapy monitoring, Eur J Nucl Med Mol Imaging (2010) 37:1643–1653 DOI 10.1007/s00259-010-1466-5.
18. Brambilla M, Matheoud R, Secco C, et al. Impact of target-to-background ratio, target size, emission scan duration, and activity on physical figures of merit for a 3D LSO-based whole body PET/CT scanner. Med Phys. 2007;34:3854-65.
19. Zorz A, Matheoud R, Richetta E, Baichoo S, Poli M, Scaggion A et al. Performance evaluation of a new time of flight PET/CT scanner: Results of a multicenter study. Phys Med 2019;68:146-154. doi: 10.1016/j.ejmp.2019.11.017.
20. Ingenuity TF PET/CT Performance Testing Technical Manual. 459800090571 Revision G, Koninklijke Philips N.V.
21. Philips NM Clinical Science, Enhanced lesion detectability and accurate quantitative imaging, White Paper, Philips Healthcare, USA.

22. Kleinbaum DG, Kupper LL and K. E. Muller, Applied Regression Analysis and Other Multivariable Methods PWS-KENT, Boston, Massachusetts, 1988
23. Council Directive 2013/59/Euratom of 5 December 2013 laying down basic safety standards for protection against the dangers arising from exposure to ionising radiation, and repealing Directives 89/618/Euratom, 90/641/Euratom, 96/29/Euratom, 97/43/Euratom and 2003/122/Euratom, 2013. http://data.europa.eu/eli/dir/2013/59/oj

Figures

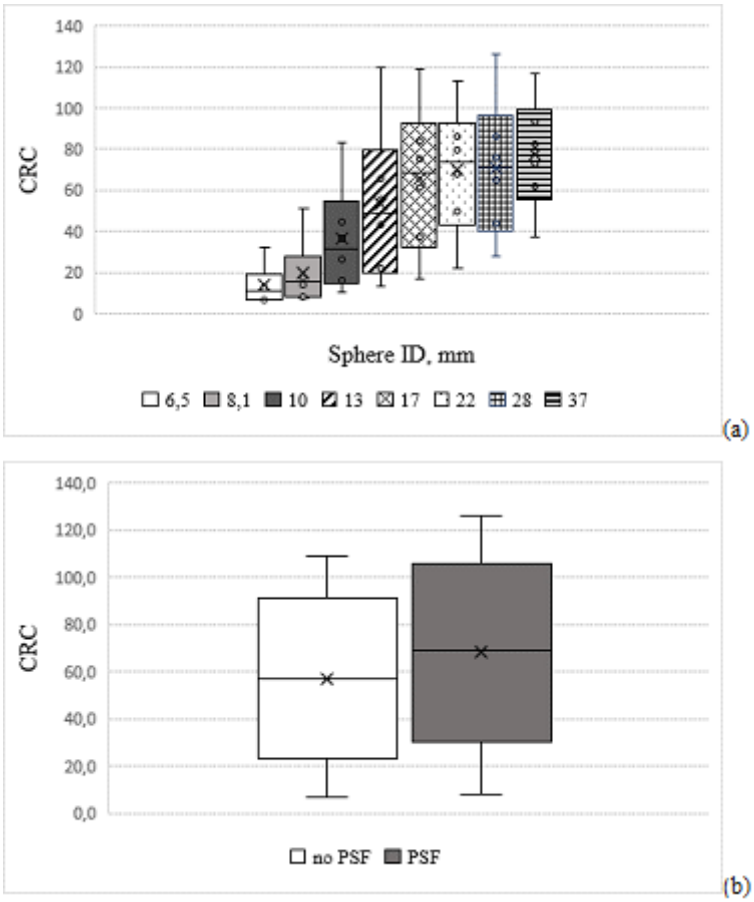

Figure 1

Box plots of CRC values as function of sphere ID (a) and PSF (b).

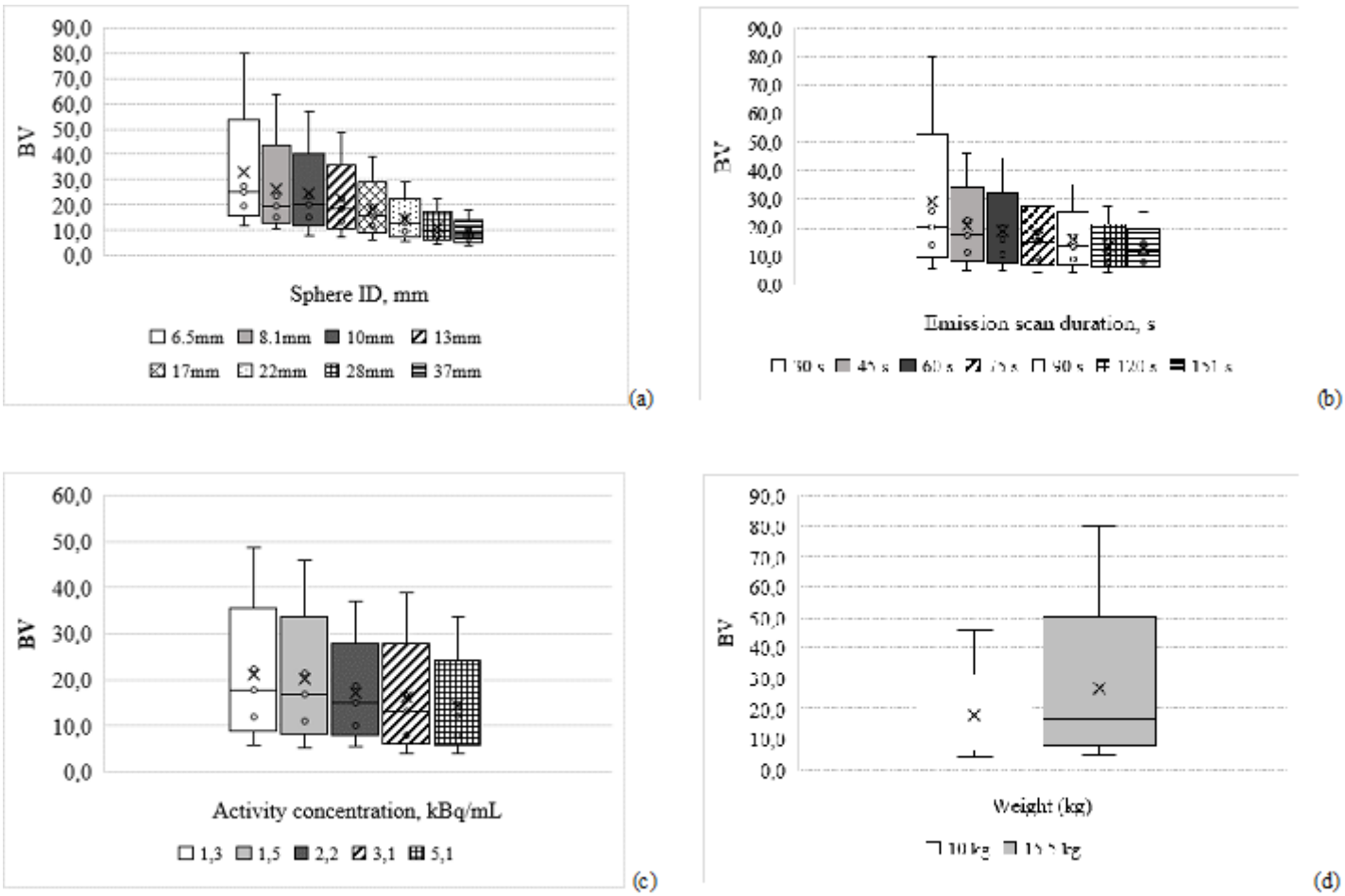

Figure 2

Box plots of BV as function of sphere ID (a), ESD (b), AC (c) and W (d).

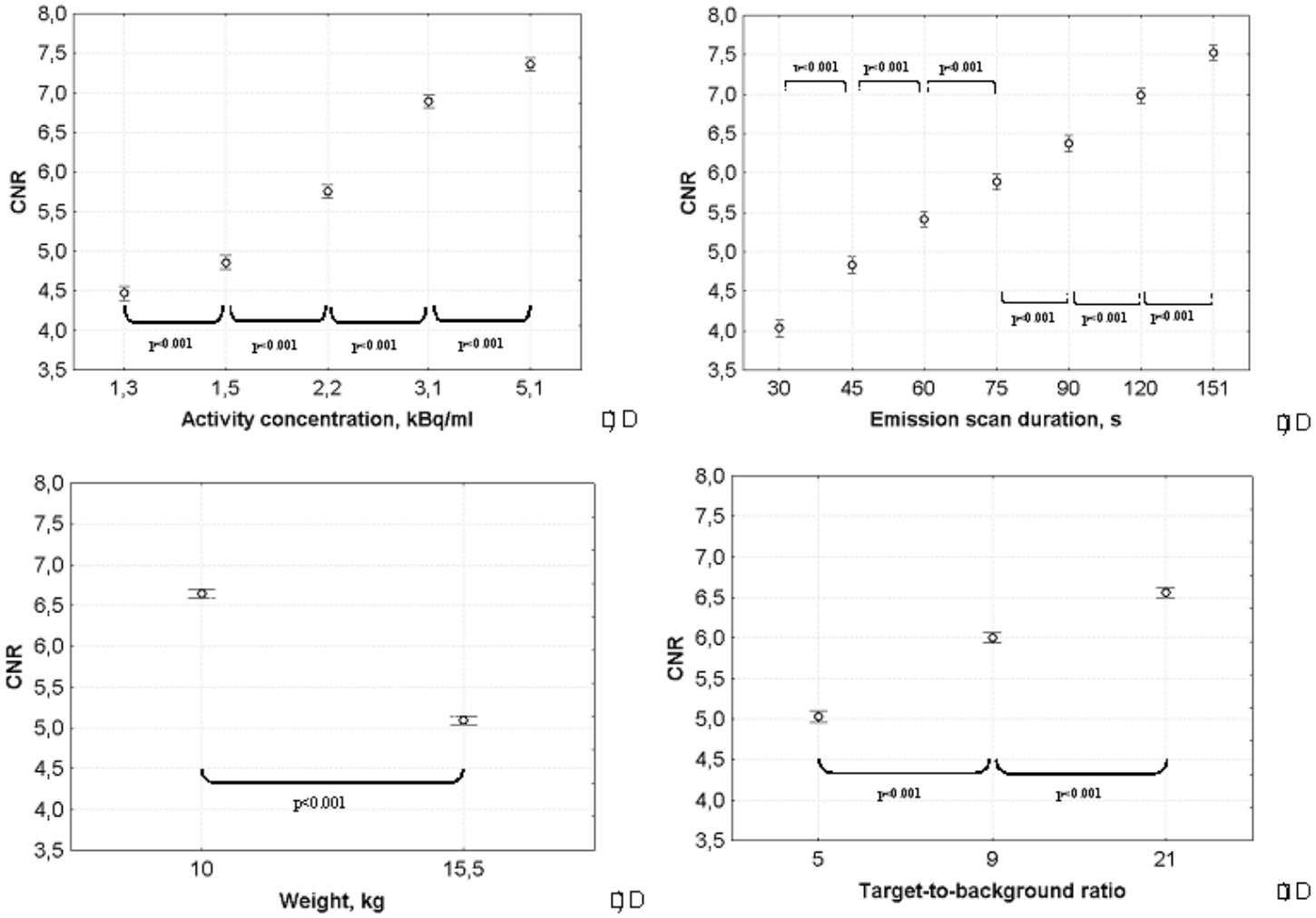

Figure 3

CNR as a function of AC (a), ESD (b), W (c) and TBR (d). Points represent least square averages; vertical bars represent 95% confidence intervals.

a)

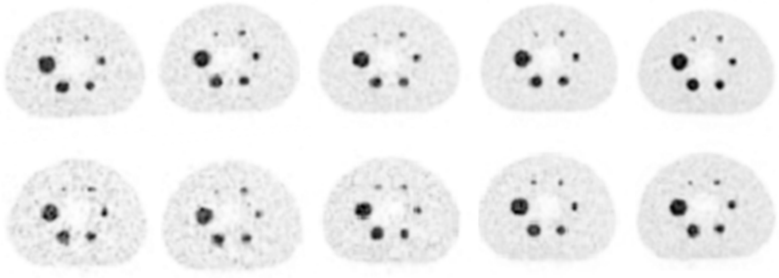

b)

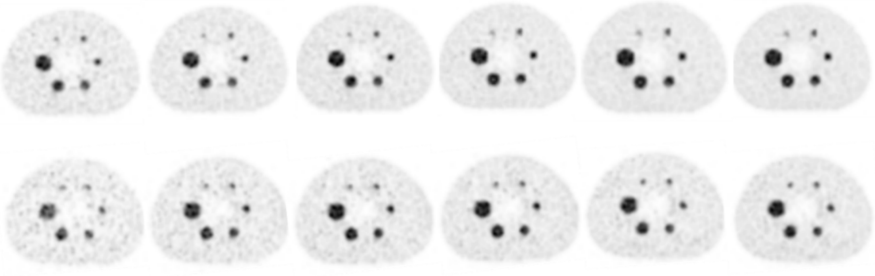

Figure 4

(a) IEC (upper row) and b-IEC (lower row) images of TBR=9 for increasing AC (from left to right) for ESD=60s. (b) IEC (upper row) and b-IEC (lower row) images of TBR=9 for increasing ESD (from left to right) for AC=2.0 kBq/ml.